


Identifying an oligodendrocyte enhancer that regulates *Olig2* expression

Chuangdong Fan^{1,†}, Dongkyeong Kim^{1,2,†}, Hongjoo An and Yungki Park ^{1,*}

¹Institute for Myelin and Glia Exploration, Department of Biochemistry, Jacobs School of Medicine and Biomedical Sciences, State University of New York at Buffalo, Buffalo, NY 14203, USA

²Present address: Department of Molecular Pharmacology, Albert Einstein College of Medicine, Bronx, NY 10461, USA.

*To whom correspondence should be addressed. Tel: +1-716-881-7579; Fax: +1-716-849-6651; Email: yungkipa@buffalo.edu

†Equal contribution

Abstract

Olig2 is a basic helix–loop–helix transcription factor that plays a critical role in the central nervous system. It directs the specification of motor neurons and oligodendrocyte precursor cells (OPCs) from neural progenitors and the subsequent maturation of OPCs into myelin-forming oligodendrocytes (OLs). It is also required for the development of astrocytes. Despite a decade-long search, enhancers that regulate the expression of *Olig2* remain elusive. We have recently developed an innovative method that maps promoter–distal enhancers to genes in a principled manner. Here, we applied it to *Olig2* in the context of OL lineage cells, uncovering an OL enhancer for it (termed *Olig2*-E1). Silencing *Olig2*-E1 by CRISPRi epigenome editing significantly downregulated *Olig2* expression. Luciferase assay and ATAC-seq and ChIP-seq data show that *Olig2*-E1 is an OL-specific enhancer that is conserved across human, mouse and rat. Hi-C data reveal that *Olig2*-E1 physically interacts with *OLIG2* and suggest that this interaction is specific to OL lineage cells. In sum, *Olig2*-E1 is an evolutionarily conserved OL-specific enhancer that drives the expression of *Olig2*.

Introduction

During embryonic development, *Olig2* is turned on in neural progenitors for their specification into motor neurons and oligodendrocyte precursor cells (OPCs) (1–4). *Olig2* continues to be expressed in OPCs, getting them ready for differentiation into myelin-forming oligodendrocytes (OLs) (5–7). Interestingly, the deletion of *Olig2* in differentiating OLs accelerates their differentiation and myelination (8), illustrating the stage-specific opposing effects of *Olig2* on OL maturation. *Olig2* also plays an important role in the development of astrocytes (9–11). Mechanistically, *Olig2* is a basic helix–loop–helix transcription factor that forms dimers with itself or other transcription factors to exert regulatory effects on gene expression (12), activating and repressing it in a context-specific manner (5,6,13).

Olig2 is a dosage-sensitive gene, as evidenced by Down syndrome (also known as trisomy 21). *OLIG2* is in chromosome 21, and thus, its gene dosage in Down syndrome patients is three. The increased expression of *OLIG2* is thought to cause the imbalance between excitatory and inhibitory tones in the central nervous system (CNS) (14–16), leading to cognitive deficits. In organoids and animal models, it was possible to restore cellular and behavioral impairments by lowering the expression of *OLIG2* (14,16). Clearly, the right level of *Olig2* expression is indispensable for the development and function of the CNS.

Cell type-specific gene expression is coordinated by transcription factors acting on the gene's enhancers (cis-regulatory DNA elements). Thus, in order to understand *Olig2* expression, one

has to identify its enhancers and transcription factors acting on them. Logically, enhancer identification would come first because, without the knowledge of enhancers, it would not be feasible to identify transcription factors acting on them. A common feature of enhancers is that they can be anywhere with regard to target genes (17,18)—far upstream, near upstream, in gene body, near downstream or far downstream. This makes it a formidable challenge to map out enhancers for a gene of interest. For this reason, enhancers that govern *Olig2* remain to be identified despite a decade-long search (19–21). We have recently developed an innovative method that links enhancers to target genes in a principled manner (22). Its power has been demonstrated for *Myrf* (22), *Rgcc* (23) and *Plp1* (24). Here, we applied it to *Olig2* in the context of OL lineage cells, uncovering an evolutionarily conserved OL enhancer for it.

Results

Overview: a principled method to find OL enhancers for *Olig2*

In this section, we provide an overview of our new enhancer-mapping method, as applied to *Olig2* (Fig. 1). The following sections give the detailed description of each step and actual data. The enhancer-mapping method consists of three steps. First, chromatin interaction studies have shown that a gene and its enhancer tend to be found in the same topologically associating domain (TAD), a fundamental unit of genome organization

Received: July 2, 2022. Revised: September 26, 2022. Accepted: September 30, 2022

© The Author(s) 2022. Published by Oxford University Press. All rights reserved. For Permissions, please email: journals.permissions@oup.com

This is an Open Access article distributed under the terms of the Creative Commons Attribution Non-Commercial License (<http://creativecommons.org/licenses/by-nc/4.0/>), which permits non-commercial re-use, distribution, and reproduction in any medium, provided the original work is properly cited. For commercial re-use, please contact journals.permissions@oup.com

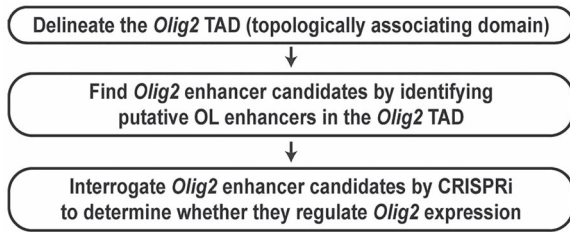


Figure 1. A principled method to find OL enhancers for *Olig2*.

and function (25,26). Thus, the TAD where *Olig2* belongs is where we should look in search of *Olig2* enhancers. Of note, the internal detail of a TAD reflects cell type-specific gene-enhancer interactions, differing between cell types. In contrast, the boundary of a TAD tends to be conserved between cell types and species (25,27). This enabled us to delineate TADs for OL genes by analyzing chromatin interaction data for non-OL cell types (22–24). Now, OL chromatin interaction data are publicly available (28), aiding TAD analysis for OL genes (24). Second, we systematically identify putative OL enhancers in the *Olig2* TAD (Fig. 1), which are qualified to be *Olig2* enhancer candidates (ECs) because they are in the same TAD as *Olig2*. Our previous study generated a genome-wide map of putative OL enhancers by integrating OL ChIP-seq data (22). We compare this genome-wide map with the *Olig2* TAD, finding all putative OL enhancers in the *Olig2* TAD. Third, we interrogate *Olig2* ECs with CRISPRi, a state-of-the-art epigenome editing method (29–33), to determine whether they regulate *Olig2* expression. CRISPRi potentially silences promoters and enhancers in the genomic context (29–33), providing a revolutionary way to link enhancers to target genes and vice versa.

TAD analysis for *Olig2*

To define the *Olig2* TAD, we explored public Hi-C data for 6 diverse human cell types (IMR90, K562, HMEC, HUVEC, NHEK and OL) (26,28). *OLIG2* is on the plus strand of chromosome 21. The location of the *OLIG2* promoter is indicated by thin crossing lines in Figure 2. In each panel, the diagonal represents the genome. Off the diagonal, the interaction strength between two loci is indicated by red tone where white means no interaction. The Hi-C data show that *OLIG2* belongs to a TAD that spans 390 Kb (210 Kb upstream and 180 Kb downstream of *OLIG2*; marked in blue in Fig. 2H). As expected, the *OLIG2* TAD boundary is conserved across the six cell types, while its internal detail is not (Figs. 2A–F). To check whether the *OLIG2* TAD is conserved in mouse, we examined the Hi-C data for CH12-LX (B cell lymphoma) (26). As in the human genome, *Olig2* is on the plus strand in the mouse genome. The CH12-LX Hi-C data reveal that the *Olig2* TAD (marked in blue in Fig. 2I) is the same as the *OLIG2* one, as evident from the relative locations of the TAD boundary and nearby genes (*PAXBP1* and *IFNAR2* in Fig. 2H and *Paxbp1* and *Ifnar2* in Fig. 2I). Of note, the *Olig2* TAD is smaller than the human counterpart because the mouse genome is smaller than the human one. This comparative analysis highlights the remarkable evolutionary conservation of the *OLIG2* TAD, supporting the idea that critical *Olig2* enhancers would be found in the *Olig2* TAD.

Identification and CRISPRi analysis of *Olig2* ECs

Our genome-wide map of putative OL enhancers (22) disclosed 5 putative OL enhancers in the *Olig2* TAD (EC1–5 in Fig. 3A). Since they are in the same TAD as *Olig2*, they are qualified to be *Olig2* ECs. They were ranked based on the strength of the

underlying data, with EC1 and EC5 being the best and worst ECs, respectively. We checked whether there is any overlap between them and putative regulatory elements around *Olig2* analyzed by previous studies. The K23 enhancer found by Sun and coworkers does not match any of the five ECs (19). Of the 10 putative enhancers considered by Chen and colleagues, the 8th one (mm8 chr16:91080626–91082625 in their Table 2) overlaps EC2 (20); there is no overlap for the other 9. None of the three enhancers discovered by Friedli and coworkers matches the five ECs (21). In sum, EC2 is the only EC that was studied by the previous studies. EC1 (our top EC) has never been examined for *Olig2*.

We interrogated the five ECs with CRISPRi to find those that regulate *Olig2* expression. In CRISPRi, dCas9-KRAB, a fusion protein between a nuclease-null Cas9 (dCas9) and a KRAB domain, is targeted to a specific locus by guide RNAs (gRNAs). When targeted to a promoter, dCas9-KRAB silences it by inducing trimethylation of H3K9 (K9 of histone 3) (29–33). When targeted to an enhancer, dCas9-KRAB silences it by the same mechanism (31–33), which in turn downregulates its target genes. This is how one can map enhancers to target genes by CRISPRi. Since enhancers are bound by transcription factors, they are usually depleted of nucleosomes. Hence, although H3K27ac is known to mark active enhancers, its enrichment is found in the shoulders flanking an enhancer rather than in the enhancer itself. This is why a peak-valley-peak pattern is observed for enhancers in H3K27ac ChIP-seq data (an example shown in Fig. 3C). Guided by this principle, we identified core enhancer regions for the five ECs (highlighted in yellow in Fig. 3B). For EC1 and EC2, there seems to be two core enhancer regions (marked as A and B in Fig. 3B), and we tested both. Altogether, 7 putative enhancers were examined for *Olig2* (EC1A, EC1B, EC2A, EC2B, EC3, EC4 and EC5).

To silence an *Olig2* EC, dCas9-KRAB was targeted to it by 4 independent gRNAs (G1–4) in Oli-neu cells, a widely used mouse OL cell line (37). Specifically, gRNAs were cloned into an in-house piggyBac-based plasmid and integrated into the genome of an in-house Oli-neu cell line that expresses dCas9-KRAB in a doxycycline-dependent manner. In resulting cell lines, gRNAs were expressed constitutively, while the expression of dCas9-KRAB was induced by doxycycline. As negative controls, two Oli-neu cell lines were generated in parallel, where *Scr1* and *Scr2*, two non-targeting gRNAs, were integrated into the genome. Two gRNAs that deliver dCas9-KRAB to the *Olig2* promoter (Pro1 and Pro2) were used for positive control cell lines. Oli-neu cell lines were cultured in the proliferation condition for 2 days in the presence of doxycycline before RNA extraction.

For EC1, RT-qPCR showed that EC1B is the region that works as an enhancer for *Olig2* (Fig. 4A); all four gRNAs for EC1B came out positive. To corroborate these results, we retested EC1A and EC1B with more gRNAs in a luciferase assay that utilizes *Olig2*LR5, an in-house *Olig2* luciferase reporter that was generated by cloning an *Olig2* ChIP-seq peak (rn4 chr12:21433840–21434301) (6) into pGL3-promoter. Its characterization is available in Supplementary Material, Figure S1. When *Olig2* was knocked down by CRISPRi, the reporter activity of *Olig2*LR5 went up significantly (Pro1 in Fig. 4B), showing that *Olig2* works as a repressor for it. The same was observed when EC1B was silenced by the six gRNAs (Fig. 4B), confirming the regulatory relationship between EC1B and *Olig2* detected by RT-qPCR. In contrast, none of the 12 EC1A gRNAs elevated the reporter activity of *Olig2*LR5. To see if EC1A cooperates with EC1B in a synergistic manner, we silenced both EC1A and EC1B by co-expressing G3 of EC1A with G2 or G3 of EC1B. It did not lead to a greater knockdown of *Olig2* (Fig. 4A). In fact, the dilution effect of co-expressing two gRNAs diminished the impact of EC1B

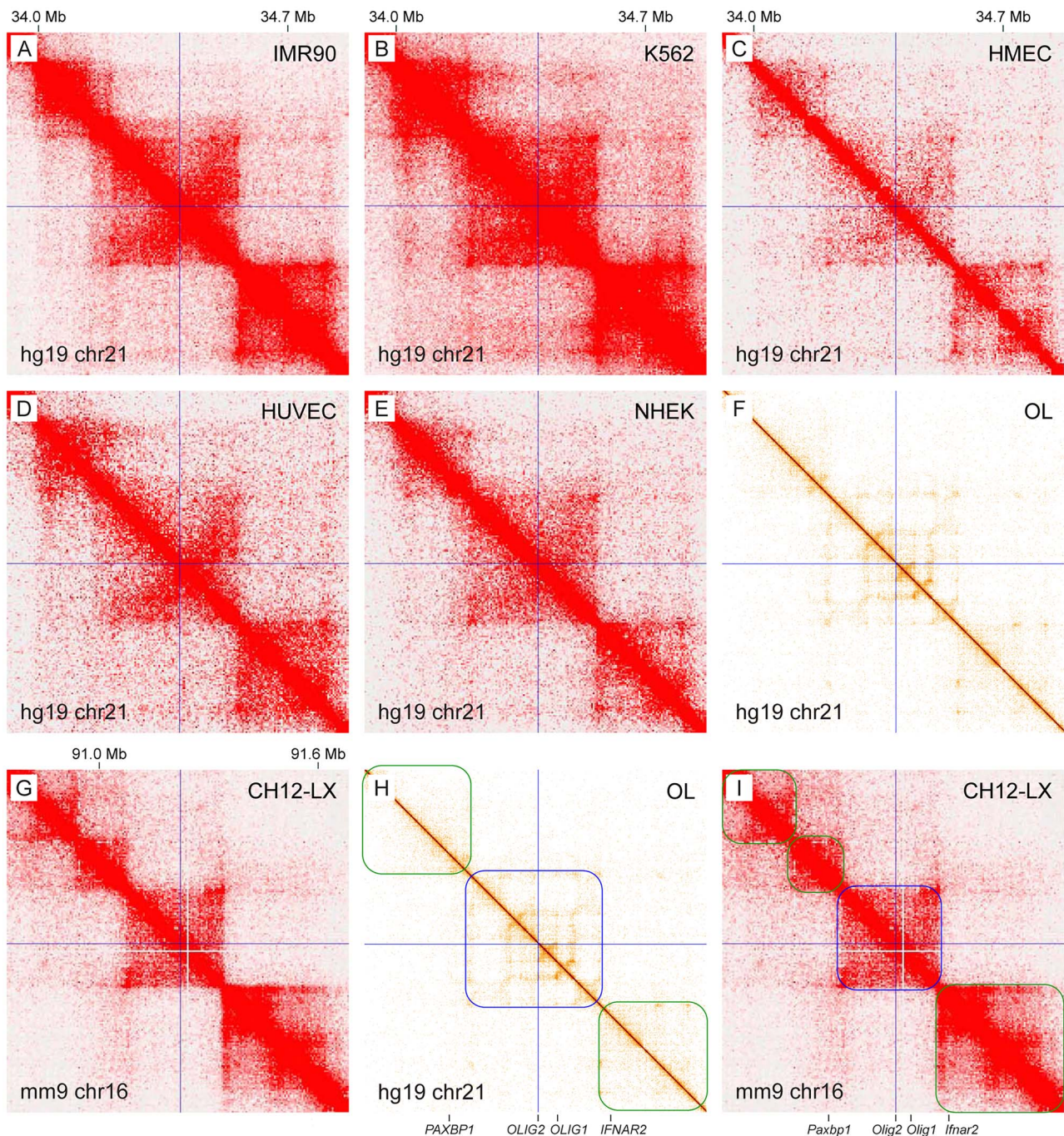


Figure 2. TAD analysis for *Olig2*. Public Hi-C data for 7 diverse cell types from human and mouse. On the diagonal is the genome. Off the diagonal, the interaction strength between two loci is indicated by red tone where white means no interaction. The *OLIG2*/*Olig2* promoter locations are marked by thin crossing lines. The *OLIG2* TAD is marked by a blue box for OLs in panel H. The corresponding TAD for *Olig2* is marked by a blue box for CH12-LX in panel I. Other potential TADs upstream and downstream of the *OLIG2*/*Olig2* TAD are marked by green boxes in panels H and I. IMR90: lung fibroblast. K562: chronic myelogenous leukemia cell. HMEC: human mammary epithelial cell. HUVEC: human umbilical vein endothelial cell. NHEK: normal human epidermal keratinocyte. CH12-LX: murine CH12 B cell lymphoma cell. These figures were prepared by using Juicebox (34,35) and HiGlass (36).

gRNAs such that there was no change in *Olig2* expression. Overall, these results demonstrate that EC1B is the core enhancer of EC1 that activates *Olig2* expression in Oli-neu cells.

EC2 is found near upstream of *Olig2* (Fig. 3A). For this reason, previous studies assumed that it would regulate *Olig2* expression (38,39). Surprisingly, all EC2 gRNAs came out negative (Fig. 4C). EC2A displays a relatively large valley of H3K27ac signals (Fig. 3B). To back up the negative RT-qPCR result for EC2A, we retested it with more gRNAs in an *Olig2*LR5-based luciferase assay. None

of the 15 EC2A gRNAs altered the reporter activity of *Olig2*LR5 (Fig. 4D). To find whether EC2A and EC2B work together in a synergistic manner, we silenced both by various gRNA combinations. The expression of *Olig2* was not affected by the 8 combinations that we tried (Fig. 4C). These results reveal that EC2 is not required for *Olig2* expression in Oli-neu cells. For EC3–5, which display only a modest level of enhancer-associated epigenetic marks, all four gRNAs came out negative (Fig. 4E). An *Olig2*LR5-based luciferase assay confirmed these results (Supplementary Material, Fig. S2).

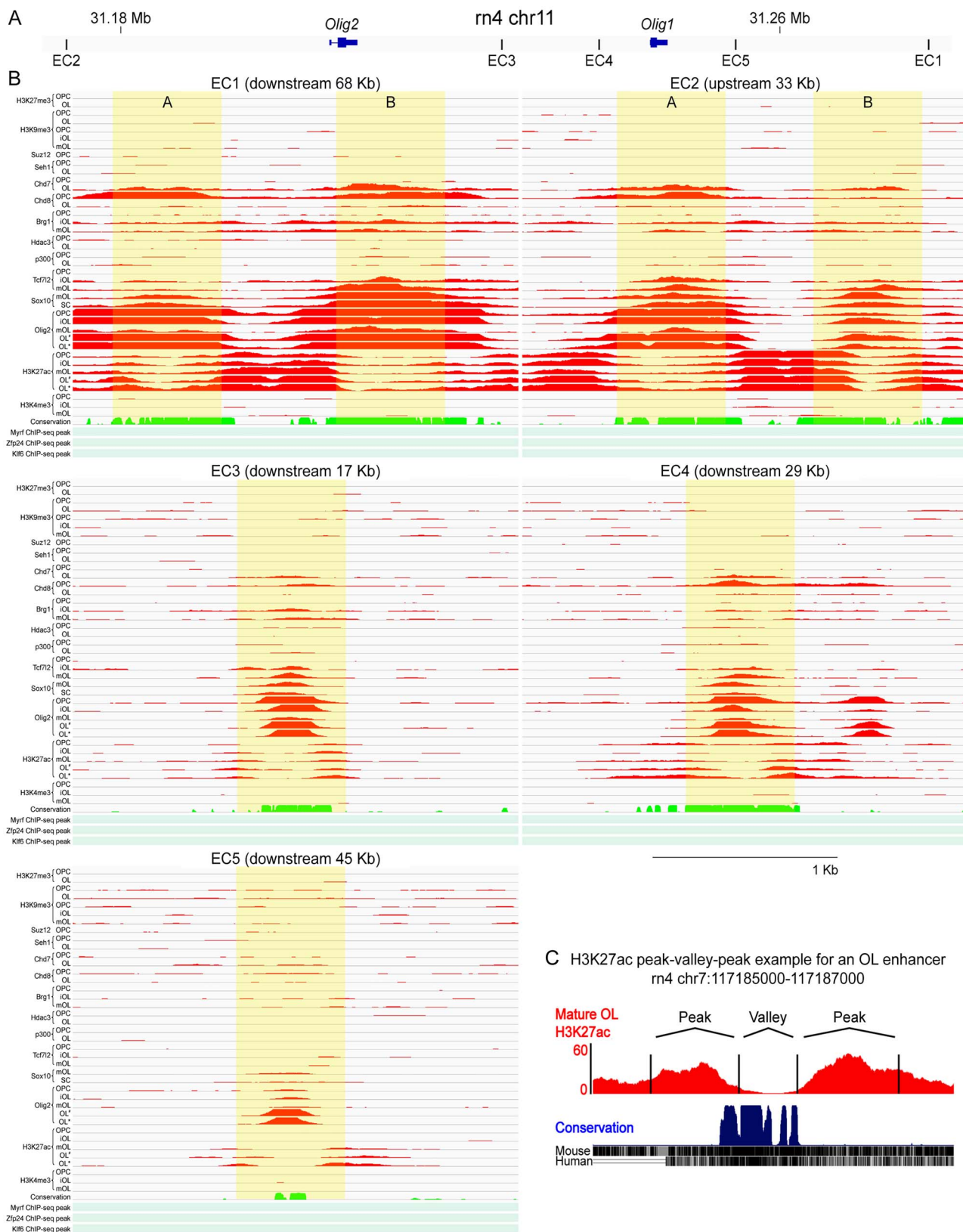


Figure 3. Five *Olig2* ECs. (A) The locations of the five *Olig2* ECs. (B) Rat OL ChIP-seq data for the five *Olig2* ECs. OPC: OL precursor cell. iOL: immature OL. mOL: mature OL. SC: spinal cord. For the Myrf ChIP-seq data, only peak locations are shown because the raw data are not available. The mouse Zfp24 and Klf6 ChIP-seq data were mapped to the rat genome by LiftOver. OL[#] and OL*_{*}: OLs treated with vehicle and lysophosphatidylcholine, respectively. Conservation: phastCons scores for the alignment of the following genomes: rat (rn4), mouse (mm8), human (hg18), dog (canFam2), cow (bosTau2), opossum (monDom4), chicken (galGal2), frog (xenTro1) and zebrafish (danRer3). (C) An exemplary peak-valley-peak pattern for an enhancer in H3K27ac ChIP-seq data.

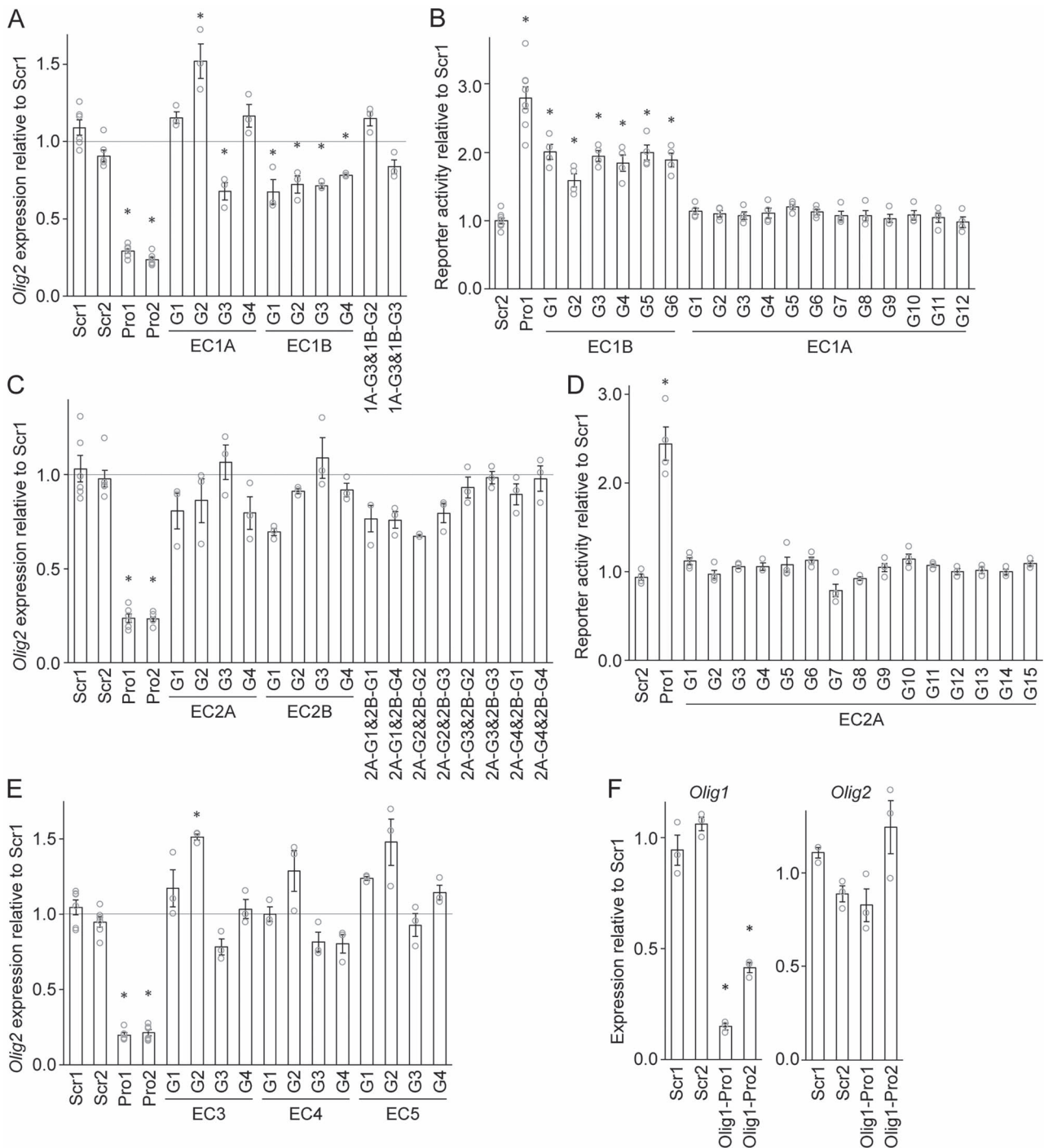


Figure 4. CRISPRi interrogation of the five *Olig2* ECs. **(A)** RT-qPCR analysis of EC1A and EC1B. Shown are data points and their mean and standard error. $*P < 4.72 \times 10^{-2}$ by Student's *t* test with Bonferroni correction. **(B)** Luciferase assay for EC1A and EC1B with Olig2LR5. Shown are data points and their mean and standard error. $*P < 1.16 \times 10^{-3}$ by Student's *t* test with Bonferroni correction. **(C)** RT-qPCR analysis of EC2A and EC2B. Shown are data points and their mean and standard error. $*P < 8.81 \times 10^{-6}$ by Student's *t* test with Bonferroni correction. **(D)** Luciferase assay for EC2A with Olig2LR5. Shown are data points and their mean and standard error. $*P < 3.55 \times 10^{-3}$ by Student's *t* test with Bonferroni correction. **(E)** RT-qPCR analysis of EC3-5. Shown are data points and their mean and standard error. $*P < 5.02 \times 10^{-3}$ by Student's *t* test with Bonferroni correction. **(F)** RT-qPCR analysis of the *Olig1* promoter. Shown are data points and their mean and standard error. $*P < 1.01 \times 10^{-2}$ by Student's *t* test with Bonferroni correction.

Some promoters work as enhancers (40). *Olig1* is found in the *Olig2* TAD (Fig. 2), and we wondered whether the *Olig1* promoter acts as an *Olig2* enhancer. To test this idea, we silenced the *Olig1* promoter by two different gRNAs. RT-qPCR showed that *Olig1* was successfully knocked down, yet there was no change in *Olig2* expression (Fig. 4F). These results argue that the *Olig1* promoter does not potentiate *Olig2* transcription.

So far, all epigenome editing experiments were performed with Oli-neu cells, a model cell line for OL lineage cells. To determine whether EC1B also controls *Olig2* expression in primary OPCs, we repeated the CRISPRi experiment with mouse OPCs purified by immunopanning (41,42). Transfection efficiency for mouse OPCs is neither high enough for RT-qPCR nor is it possible to subject them to a drug selection process. Thus, we had to resort

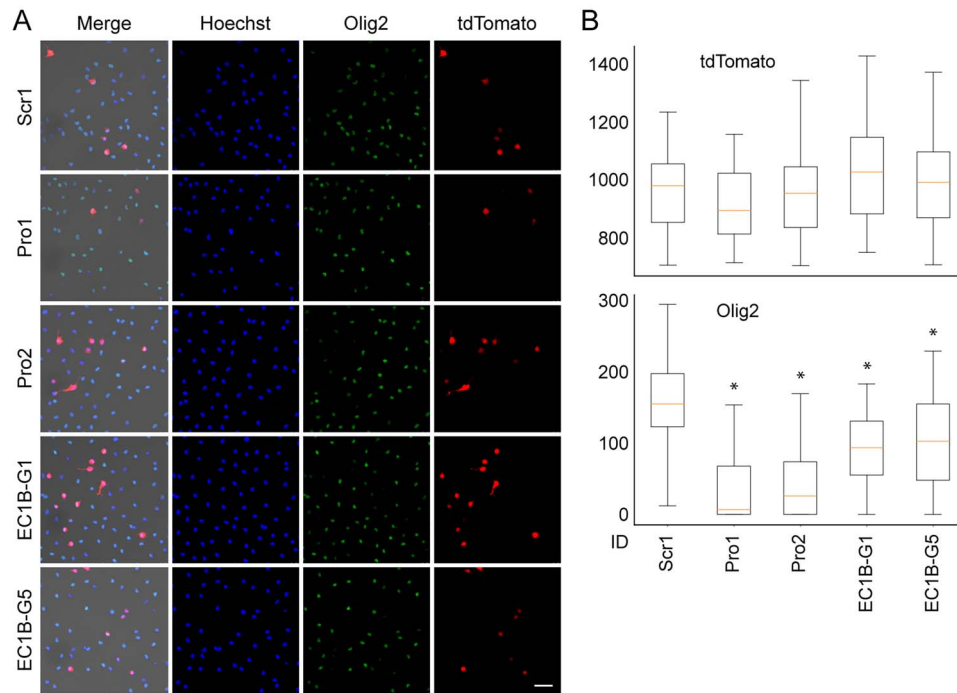


Figure 5. Interrogation of EC1B with mouse OPCs. (A) Quantitative immunofluorescence of Olig2 in mouse OPCs after CRISPRi. Shown are representative images for the five gRNAs. For each gRNA, 31 pictures were taken and analyzed. Scale bar, 50 μ m. (B) Signal quantification for individual cells by CellProfiler. * $P < 3.27 \times 10^{-8}$ by Student's t test with Bonferroni correction. ID: integrated signal density.

to quantitative immunofluorescence where individual cells are analyzed and thus high transfection efficiency is not required. A plasmid expressing dCas9-KRAB and tdTomato was transfected into mouse OPCs, together with gRNA plasmids. Transfected OPCs were cultured in the proliferation condition for 2 days. They were stained for Olig2 and tdTomato (identifying transfected cells). Olig2 and tdTomato signals were quantified for individual OPCs by CellProfiler (43). This quantitative image analysis revealed that while tdTomato signals were comparable across the samples, Olig2 signals were much lower when dCas9-KRAB was targeted to the *Olig2* promoter (Pro1 and Pro2, Fig. 5A and B) or EC1B (EC1B-G1 and EC1B-G5, Fig. 5A and B). These results demonstrate that the regulatory control of EC1B over *Olig2* holds true in primary OPCs, too.

EC1B is a conserved OL-specific enhancer

The epigenetic features (Fig. 3B) and the epigenome editing results (Figs 4 and 5) strongly suggest that EC1B works as an enhancer in OL lineage cells. Consistently, EC1B is well conserved at the nucleotide level (Fig. 3B). To confirm the OL enhancer activity of EC1B, we performed a luciferase assay. EC1B (mm9 chr16:91305254–91306767) was cloned into pGL3-promoter and transfected into OPCs purified from rat brain by immunopanning. Transfected OPCs were cultured in the proliferation condition for 2 days. EC1B exhibited a strong enhancer activity in them (Fig. 6A). In this analysis, pGL3-promoter (empty vector) was used to estimate baselines. Since our data indicate that EC1B is an OL enhancer that governs *Olig2*, it will henceforth be referred to as *Olig2*-E1.

To elucidate the property of *Olig2*-E1, we surveyed public data. First, we analyzed the human brain single-nucleus ATAC-seq data from Swarup and colleagues (44). We calibrated it with the loci of *GAPDH* and *ACTB* for a quantitative comparison of peak heights among different cell types. The single-nucleus ATAC-seq data

show that *Olig2*-E1 is open in OL lineage cells (OPC and OL, Fig. 6B). Furthermore, it reveals that *Olig2*-E1 is specific to OL lineage cells. Second, we looked up the human brain cell type-specific ChIP-seq and ATAC-seq data from Glass and co-workers (45). We calibrated these data in the same manner. *Olig2*-E1 squarely coincides with the valley of an H3K27ac peak-valley-peak and an ATAC-seq peak in OL lineage cells (Fig. 6B). Consistent with the Swarup data, *Olig2*-E1 is active only in OL lineage cells. Third, to check the specificity of *Olig2*-E1 more broadly, we inquired the H3K27ac ChIP-seq data from the NIH Roadmap Epigenomics Project (46), which were calibrated in the same manner. It points out that *Olig2*-E1 is active only in the brain tissues (Supplementary Material, Fig. S3), supporting its OL specificity. Of note, there is no spinal cord H3K27ac data in the Roadmap Epigenomics Project. Finally, we explored the mouse single-cell ATAC-seq data from Shendure and colleagues, which were clustered into 21 cell types and calibrated in the same way (47). This dataset does not have data for OPCs. It shows that *Olig2*-E1 is active only in OLs (Fig. 6C). Taken together, *Olig2*-E1 is an OL-specific enhancer that is conserved across human, mouse and rat.

Olig2-E1 interacts with the *OLIG2* promoter

The internal detail of a TAD reflects cell type-specific gene-enhancer interactions. Thus, from the OPC and OL Hi-C data (28), we may be able to detect an OL-specific chromatin interaction between *Olig2*-E1 and *OLIG2*. Since the pro-differentiation effect of *Olig2* on OL lineage cells is most prominent in the OPC stage (5,8), our study of *Olig2*-E1 has been in the context of proliferating OL lineage cells and OPCs. In this regard, it would be desirable to analyze a Hi-C data for OPCs to see if *Olig2*-E1 physically interacts with *OLIG2* in OPCs. Unfortunately, the OPC Hi-C data are extremely sparse and cannot be used for this purpose (see below) (28). This is why we turned to the OL Hi-C data (28), which is deep enough to divulge the internal architecture of OL TADs. Although less ideal,

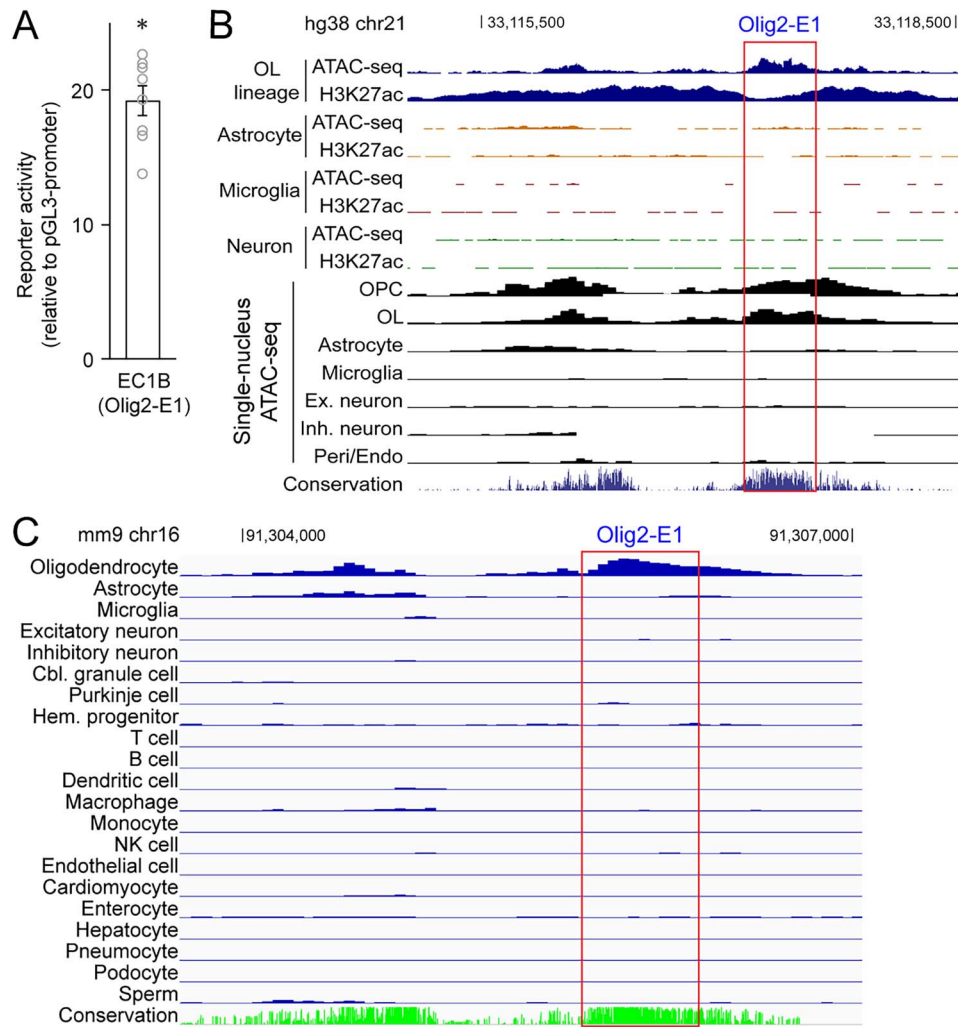


Figure 6. EC1B (Olig2-E1) is a conserved OL-specific enhancer. **(A)** Luciferase assay for EC1B (Olig2-E1) in rat OPCs cultured in the proliferation condition. Shown are data points and their mean and standard error. $*P < 7.79 \times 10^{-7}$ by Student's *t* test. **(B)** Human brain ATAC-seq and ChIP-seq data for Olig2-E1. Ex.: Excitatory. Inh.: Inhibitory. **(C)** Mouse single-cell ATAC-seq data for Olig2-E1. Cbl.: Cerebellar. Hem.: Hematopoietic.

the OL data are still useful and relevant because Olig2-E1 is active in both OPCs and OLs (Fig. 6B). The OL Hi-C data reveal a strong interaction between Olig2-E1 and *OLIG2* (traced by thin lines in Fig. 7A). To gauge its genome-wide significance, all pairs of loci in the genome that are equidistant apart were examined. The interaction strength between Olig2-E1 and *OLIG2*, which are 92 Kb apart, is 0.0024 (see Materials and Methods). There are 303 381 pairs of loci that are equidistant apart in the OL Hi-C data (Fig. 7B). Of these, 825 pairs physically interact, and the pair of Olig2-E1 and *OLIG2* exhibit the 47th strongest interaction. Clearly, it is a highly significant interaction from the genome-wide perspective.

To assess the OL specificity of the interaction between Olig2-E1 and *OLIG2*, we surveyed non-OL Hi-C data. For this analysis, one would normalize multiple Hi-C data in such a way that interaction strengths calculated from different Hi-C data can be directly compared. Although such normalization method is available (48), it is impractical because many Hi-C data are extremely sparse. Therefore, we had to proceed in an indirect manner. For the 6 sparse datasets (OPC, Astrocyte, Microglia, HMEC, HUVEC and NHEK), Olig2-E1 does not interact with *OLIG2* (Fig. 7B). This may well be because they are sparse. Therefore, we cannot draw any conclusions from them. For the remaining four datasets that are as deep as the OL one, either there is no interaction (KBM7), or the

interaction is not as strong as in OLs rank wise (GM12878, IMR90 and K562). It is reasonable to assume that a comparable number of gene-enhancer interactions sustain OLs and the latter three cell types. In OLs, the interaction between Olig2-E1 and *OLIG2* is the 47th strongest, while it is beyond the 880th for them. This observation suggests that the interaction of Olig2-E1 with *OLIG2* is specific to OLs. The OL-specific interaction between Olig2-E1 and *OLIG2* is consistent with the OL-specific enhancer activity of Olig2-E1 shown in Figure 6.

Discussion

Olig2 is a master regulator for the development and function of the CNS. Nonetheless, enhancers that govern *Olig2* expression remain poorly understood. Our study has identified a long-sought OL enhancer for it, which we named Olig2-E1. It is located 77 Kb downstream of *Olig2* and does not match any of the regulatory elements inspected by previous studies (19–21). Since Olig2 is required for OL myelination, we expect Olig2-E1 to play an important role in it. To test this hypothesis, we plan to generate mutant mice where Olig2-E1 is flanked by loxP sequences for conditional knockout. Although we discovered Olig2-E1 in the context of OL lineage cells, it may also function in other contexts. For example,

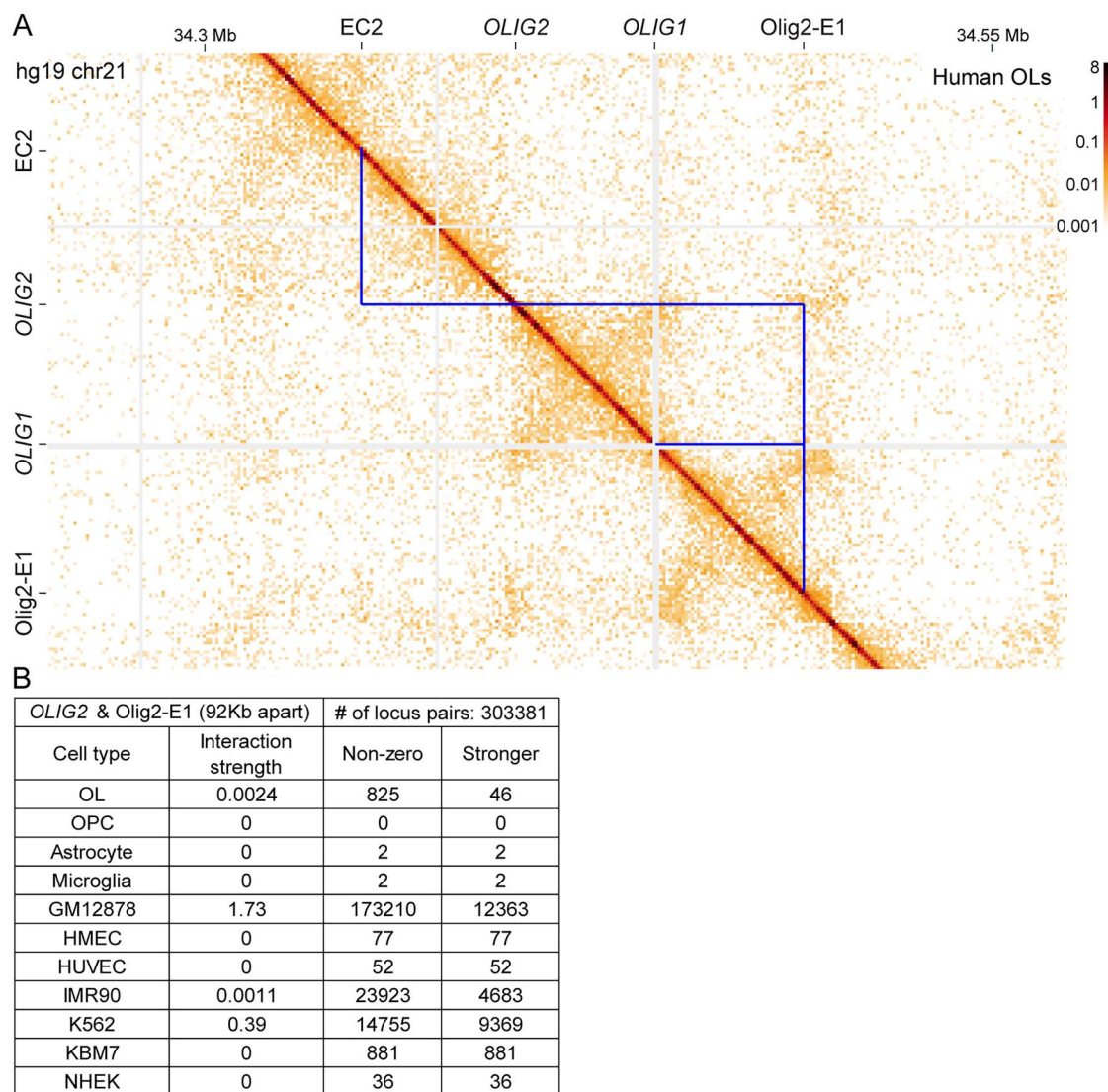


Figure 7. Chromatin interaction between Olig2-E1 and OLIG2. (A) Human OL Hi-C data zoomed in on OLIG2 and Olig2-E1. This figure was generated by using HiGlass. (B) Comparative analysis of Hi-C data for Olig2-E1 and OLIG2.

it may be important for the specification of motor neurons and OPCs from neural progenitors. In support of this prediction, we found that Olig2-E1 is highly active in neural progenitors (Supplementary Material, Fig. S4). Furthermore, a previous study found that a BAC transgene (BAC-2401C4), which does not include Olig2-E1, was not able to fully rescue Olig2 expression in Olig2 null mice for motor neurons and OL lineage cells (19).

Gene expression is coordinated by positive and negative regulators acting on the gene's enhancers. Thus, we can find upstream regulators of Olig2 by identifying transcription factors that act on Olig2-E1. The ChIP-seq data (Fig. 3B) indicate that Olig2 avidly binds to Olig2-E1 in OPCs (6), prompting us to hypothesize that Olig2 self-regulates its expression by acting on Olig2-E1. To our disappointment, we failed to obtain data that support it (Supplementary Material, Fig. S5). On the one hand, it was surprising in view of the spectacular Olig2 ChIP-seq peak over Olig2-E1. On the other hand, it was not surprising because we encountered a similar situation during the development of Olig2LR5, the Olig2 luciferase reporter extensively used for the current study. To generate a sensitive luciferase reporter for Olig2, we tested 8 good-looking Olig2 ChIP-seq peaks (6). Olig2LR5 was the most

sensitive responder to Olig2, with the other 7 showing only a lukewarm response (data not shown). It is not clear why there is a poor correlation between Olig2 binding, as reflected by ChIP-seq, and Olig2 activity. As a basic helix-loop-helix transcription factor, Olig2 recognizes a relatively simple motif (CAGCTG), and it is likely to tolerate some mutations in the motif. We speculate that, perhaps because of this simplicity of the DNA motif, Olig2 may be able to bind to open chromatin (e.g. enhancers) rather indiscriminately. In line with this speculation, Olig2 binds to more than 20 000 loci in OL lineage cells (6). It is also interesting to note that Olig2-E1 lacks a canonical CAGCTG motif incidence, unlike Olig2LR5.

To find upstream regulators of Olig2, we plan to perform a CRISPRi screen where a candidate transcription factor is knocked down by CRISPRi and its impact on the enhancer activity of Olig2-E1 measured by luciferase assay. Since a balance between positive and negative regulators would fine-tune the expression of Olig2, it would be meaningful to identify both classes of regulators. Equally important would be the mapping of their binding sites in Olig2-E1. For example, mutations of a binding site for a negative regulator may upregulate OLIG2 expression, potentially providing

a rational explanation for those intellectual disability cases where *OLIG2* is overexpressed without chromosome 21 trisomy.

Unexpectedly, our epigenome editing analysis revealed that EC2 does not regulate *Olig2*. To arrive at this conclusion, we tested as many as 19 gRNAs (15 for EC2A and 4 for EC2B). In agreement with the dispensability of EC2 for *Olig2* expression, the human OL Hi-C data show that EC2 does not interact with *OLIG2* (Fig. 7A). This is in sharp contrast to its strong interaction with *Olig2*-E1, despite the fact that it is much closer to EC2 than to *Olig2*-E1 (Fig. 3A). It remains to be elucidated whether EC2 works as an enhancer in other contexts.

Olig1 is in the same TAD as *Olig2* (Fig. 2). We found that *Olig2*-E1 is required for *Olig1* expression in Oli-neu cells (Supplementary Material, Fig. S6A), suggesting that *Olig2*-E1 also governs *Olig1* in OL lineage cells. Consistent with this possibility, *Olig2*-E1 significantly interacts with *OLIG1* in human OLs (Fig. 7A). A quantitative analysis for this physical interaction is shown in Supplementary Material, Figure S6B. Unfortunately, for technical reasons, we could not validate this interesting finding with mouse OPCs. We will directly test it once we make conditional knockout mice for *Olig2*-E1.

Materials and Methods

CRISPRi constructs dCas9-KRAB was amplified from pHAGE EF1 α dCas9-KRAB (Addgene 50919) and inserted, together with an IRES (internal ribosome entry site)-tdTomato cassette, into pCAG-Cre (Addgene 13775) after the Cre was removed. This construct, which is called 'dCas9-KI', was used for quantitative immunofluorescence and luciferase assay. To generate an in-house Oli-neu cell line that expresses dCas9-KRAB in a doxycycline-dependent manner, pAAVS1-NDi-CRISPRi (Addgene 73497) was modified as follows. First, an RB (RFP and blasticidin resistance) cassette was fused to the rTA via P2A. Second, the ITRs recognized by SB100X (Addgene 34879) were inserted. This construct and SB100X were co-transfected into Oli-neu cells (37) to integrate the inducible dCas9-KRAB into the genome. To generate guide RNA (gRNA) constructs, the EF-1 α promoter of pSBbi-RN (Addgene 60519) was replaced by the sgRNA scaffold taken from lentiCRISPR v2 (Addgene 52961), and gRNAs were cloned into it. These constructs were used for quantitative immunofluorescence and luciferase assay. To generate gRNA constructs that can be integrated into the genome of Oli-neu cells, the content of PB-CA (Addgene 20960) was replaced by the sgRNA scaffold, and an GP (GFP and puromycin resistance) cassette was inserted. This construct was called 'PB-GP-U6'. gRNAs cloned into PB-GP-U6 and hypBase (49) were co-transfected into the inducible dCas9-KRAB Oli-neu cell line, and gRNA genomic insertion was selected by puromycin. The hypBase plasmid was generously provided by Breunig (50). gRNA sequences are available upon request. Sequence information for all constructs was verified by Sanger sequencing.

Animal procedures, tissue harvest, and cell culture

Animal husbandry was carried out in accordance with Institutional Animal Care and Use Committee-approved protocols. Pregnant rats were purchased from Charles River. OPCs were purified from rat and mouse pups by immunopanning (41,42). Primary OPCs and Oli-neu cells were kept in a proliferative condition by supplementing the Sato media (42) with PDGF (5 ng/mL), NT3 (5 ng/mL) and CNTF (5 ng/mL). Primary OPCs and Oli-neu cells were maintained in a humidified 5% CO₂ incubator at 37°C.

They were transfected by using Lipofectamine 2000 as per the manufacturer's instructions.

RT-qPCR

Total RNA was purified by using Trizol (ThermoFisher 15596026), and cDNA synthesized by the SuperScript First-Strand kit (Invitrogen 11904-018). Quantitative PCR was performed on C1000 Touch thermal cycler with CFX96 optical reaction module (Bio-rad). *Gapdh* was used for a loading control. Each PCR reaction contained 2 μ L of cDNA, 5 μ L of the iTaq Universal SYBR Green Supermix (Bio-rad 1725124) and 500 nM of forward and reverse primers. The primer sequences are as follows.

Gapdh (forward): GGT GAA GGT CGG TGT GAA CGG.

Gapdh (reverse): CTG GAA CAT GTA GAC CAT GTA GTT GAG G.

Olig2 (forward): CTC AAA TCT AAT TCA CAT TCG GAA GGT TGA.

Olig2 (reverse): GAC TAG ACA CCA GGC TGG C.

Olig1 (forward): CCT CGC TGT ATG AGC TGG TG.

Olig1 (reverse): TTC AGC GAG CGG AGC TTC.

Luciferase assay

*Olig2*LR5 was generated by inserting an *Olig2* ChIP-seq peak (rn4 chr12:21433840-21434301) (6) into pGL3-promoter. The mouse *Olig2*-E1 construct was generated by inserting a mouse genomic fragment (mm9 chr16:91305703-91306406) into pGL3-promoter. Luciferase assay was performed by using the Firefly and Renilla Luciferase Single Tube Assay Kit from Biotium as per the manufacturer's instructions. pRL-TK was used as an internal control. The ratio between firefly and renilla luciferase activities was taken as the reporter activity.

Immunofluorescence

Cells were fixed with 4% formaldehyde and permeabilized with 0.1% Triton X-100. Upon blocking with 1% BSA, they were incubated with primary antibodies diluted in blocking buffer at 4°C overnight, followed by incubation with fluorochrome-conjugated secondary antibodies. Nuclei were stained with Hoechst 33342 (Invitrogen H3570). Fluorescence was visualized with Leica DMi8 microscope with ORCA-Flash4.0 sCMOS camera. Reagents used for immunofluorescence are as follows: *Olig2* (Millipore MABN50), RFP (Rockland 600-401-379), donkey anti-mouse IgG, Alexa Fluor 488 (ThermoFisher A21202) and goat anti-rabbit IgG, Alexa Fluor 594 (ThermoFisher A11037).

OL ChIP-seq data

OL ChIP-seq data were downloaded from the Sequence Read Archive (SRA, <https://www.ncbi.nlm.nih.gov/sra>): GSE42454 (H3K9me3, Brg1, *Olig2*, H3K27ac, H3K4me3) (6), GSE72727 (Chd7, Sox10) (51), GSE119816 (Seh1) (52), GSE76411 (Hdac3, p300) (53), GSE82165 (Suz12) (54), GSE65119 (Tcf7l2) (55), GSE84011 (*Olig2*, H3K27ac) (56), GSE64703 (Sox10) (57), GSE107919 (Chd7, Chd8) (58), GSE101535 (Zfp24) (59) and GSE79243 (Klf6) (60). The Myrf ChIP-seq data were downloaded from the journal website (61). H3K27me3 and H3K9me3 data were kindly provided by Dr. Patrizia Casaccia (62). ChIP-seq reads were mapped to rn4 by Bowtie (63), and peaks called by MACS2 (64).

Public genomic data

Human brain single-nucleus ATAC-seq data were downloaded from the Swarup laboratory website, as indicated in the paper (44). Human brain cell type-specific ATAC-seq and ChIP-seq data from Glass and coworkers (45) are available at https://genome.ucsc.edu/s/nottalexi/glassLab_BrainCellTypes_hg19. The H3K27ac

ChIP-seq data from the Roadmap Epigenomics Project (46) were visualized by the WASHU Epigenome Browser. Mouse single-cell ATAC-seq data (47) were downloaded from the Shendure laboratory website (<https://atlas.brotmanbaty.org>). The following Hi-C data (26) were downloaded from 4DN Web Portal (<https://4dnucleome.org>): GM12878, HMEC, HUVEC, IMR90, K562, KBM7 and NHEK. The following Hi-C data (28) were downloaded from a public box directory at <https://github.com/dixonlab/scm3C-seq>: OL, OPC, Astrocyte and Microglia.

Hi-C data analysis

Cool files were analyzed by an in-house Python script that uses the cooler library (65). To compute the interaction strength between two loci, each locus was defined as a 10-Kb-long segment. The submatrix for the two loci was extracted at the resolution of 1 Kb. Most entries of submatrices are zero, even for pairs of loci that strongly interact. Thus, we removed 20 zero entries and computed the median of the remaining 80 entries, which was taken as the interaction strength. We scanned the entire human genome (hg19) for this analysis with a step size of 5 Kb.

Supplementary Material

Supplementary Material is available at HMGJ online.

Acknowledgements

National Institutes of Health [R01NS094181, R21NS102558, R21NS112608 and R21NS114476 to Y.P.]; The Legacy of Angels Foundation [to the Institute for Myelin and Glia Exploration].

References

- Lu, Q.R., Sun, T., Zhu, Z.M., Ma, N., Garcia, M., Stiles, C.D. and Rowitch, D.H. (2002) Common developmental requirement for Olig function indicates a motor neuron/oligodendrocyte connection. *Cell*, **109**, 75–86.
- Zhou, Q. and Anderson, D.J. (2002) The bHLH transcription factors OLIG2 and OLIG1 couple neuronal and glial subtype specification. *Cell*, **109**, 61–73.
- Park, H.C., Mehta, A., Richardson, J.S. and Appel, B. (2002) olig2 is required for zebrafish primary motor neuron and oligodendrocyte development. *Dev. Biol.*, **248**, 356–368.
- Takebayashi, H., Nabeshima, Y., Yoshida, S., Chisaka, O., Ikenaka, K. and Nabeshima, Y.-I. (2002) The basic helix-loop-helix factor Olig2 is essential for the development of motoneuron and oligodendrocyte lineages. *Curr. Biol.*, **12**, 1157–1163.
- Küspert, M., Hammer, A., Bösl, M.R. and Wegner, M. (2011) Olig2 regulates Sox10 expression in oligodendrocyte precursors through an evolutionary conserved distal enhancer. *Nucleic Acids Res.*, **39**, 1280–1293.
- Yu, Y., Chen, Y., Kim, B., Wang, H., Zhao, C., He, X., Liu, L., Liu, W., Wu, L.M.N., Mao, M. et al. (2013) Olig2 targets chromatin remodelers to enhancers to initiate oligodendrocyte differentiation. *Cell*, **152**, 248–261.
- Bischof, M., Weider, M., Küspert, M., Nave, K.-A. and Wegner, M. (2015) Brg1-dependent chromatin remodelling is not essentially required during oligodendroglial differentiation. *J. Neurosci.*, **35**, 21–35.
- Mei, F., Wang, H., Liu, S., Niu, J., Wang, L., He, Y., Etxeberria, A., Chan, J.R. and Xiao, L. (2013) Stage-specific deletion of Olig2 conveys opposing functions on differentiation and maturation of oligodendrocytes. *J. Neurosci.*, **33**, 8454–8462.
- Marshall, C.A., Novitsch, B.G. and Goldman, J.E. (2005) Olig2 directs astrocyte and oligodendrocyte formation in postnatal subventricular zone cells. *J. Neurosci.*, **25**, 7289–7298.
- Cai, J., Chen, Y., Cai, W.-H., Hurlock, E.C., Wu, H., Kernie, S.G., Parada, L.F. and Lu, Q.R. (2007) A crucial role for Olig2 in white matter astrocyte development. *Development*, **134**, 1887.
- Tatsumi, K., Isonishi, A., Yamasaki, M., Kawabe, Y., Morita-Takemura, S., Nakahara, K., Terada, Y., Shinjo, T., Okuda, H., Tanaka, T. et al. (2018) Olig2-lineage astrocytes: a distinct subtype of astrocytes that differs from GFAP astrocytes. *Front. Neuroanat.*, **12**, 8.
- Meijer, D.H., Kane, M.F., Mehta, S., Liu, H.Y., Harrington, E., Taylor, C.M., Stiles, C.D. and Rowitch, D.H. (2012) Separated at birth? The functional and molecular divergence of OLIG1 and OLIG2. *Nat. Rev. Neurosci.*, **13**, 819–831.
- Zhang, K., Chen, S., Yang, Q., Guo, S., Chen, Q., Liu, Z., Li, L., Jiang, M., Li, H., Hu, J. et al. (2022) The oligodendrocyte transcription factor 2 Olig2 regulates transcriptional repression during myelinogenesis in rodents. *Nat. Commun.*, **13**, 1423.
- Chakrabarti, L., Best, T.K., Cramer, N.P., Carney, R.S.E., Isaac, J.T.R., Galdzicki, Z. and Haydar, T.F. (2010) Olig1 and Olig2 triplication causes developmental brain defects in Down syndrome. *Nat. Neurosci.*, **13**, 927–934.
- Lu, J., Lian, G., Zhou, H., Esposito, G., Steardo, L., Delli-Bovi, L.C., Hecht, J.L., Lu, Q.R. and Sheen, V. (2012) OLIG2 over-expression impairs proliferation of human Down syndrome neural progenitors. *Hum. Mol. Genet.*, **21**, 2330–2340.
- Xu, R., Brawner, A.T., Li, S., Liu, J.J., Kim, H., Xue, H., Pang, Z.P., Kim, W.Y., Hart, R.P., Liu, Y. et al. (2019) OLIG2 drives abnormal neurodevelopmental phenotypes in human iPSC-based organoid and chimeric mouse models of Down syndrome. *Cell Stem Cell*, **24**, 908–926.
- Shlyueva, D., Stampfel, G. and Stark, A. (2014) Transcriptional enhancers: from properties to genome-wide predictions. *Nat. Rev. Genet.*, **15**, 272–286.
- Furlong, E.E.M. and Levine, M. (2018) Developmental enhancers and chromosome topology. *Science*, **361**, 1341–1345.
- Sun, T., Hafler, B.P., Kaing, S., Kitada, M., Ligon, K.L., Widlund, H.R., Yuk, D.-I., Stiles, C.D. and Rowitch, D.H. (2006) Evidence for motoneuron lineage-specific regulation of Olig2 in the vertebrate neural tube. *Dev. Biol.*, **292**, 152–164.
- Chen, C.T.L., Gottlieb, D.I. and Cohen, B.A. (2008) Ultraconserved elements in the Olig2 promoter. *PLoS One*, **3**, e3946.
- Friedli, M., Barde, I., Arcangeli, M., Verp, S., Quazzola, A., Zakany, J., Lin-Marq, N., Robyr, D., Attanasio, C., Spitz, F. et al. (2011) A systematic enhancer screen using lentivector transgenesis identifies conserved and non-conserved functional elements at the Olig1 and Olig2 locus. *PLoS One*, **5**, e15741.
- Kim, D., An, H., Shearer, R.S., Sharif, M., Fan, C., Choi, J.-O., Ryu, S. and Park, Y. (2019) A principled strategy for mapping enhancers to genes. *Sci. Rep.*, **9**, 11043.
- Kim, D. and Park, Y. (2019) Molecular mechanism for the multiple sclerosis risk variant rs17594362. *Hum. Mol. Genet.*, **28**, 3600–3609.
- Kim, D., An, H., Fan, C. and Park, Y. (2021) Identifying oligodendrocyte enhancers governing Plp1 expression. *Hum. Mol. Genet.*, **30**, 2225–2239.
- Dixon, J.R., Selvaraj, S., Yue, F., Kim, A., Li, Y., Shen, Y., Hu, M., Liu, J.S. and Ren, B. (2012) Topological domains in mammalian genomes identified by analysis of chromatin interactions. *Nature*, **485**, 376–380.
- Rao, S.S., Huntley, M.H., Durand, N.C., Stamenova, E.K., Bochkov, I.D., Robinson, J.T., Sanborn, A.L., Machol, I., Omer, A.D., Lander,

- E.S. et al. (2014) A 3D map of the human genome at kilobase resolution reveals principles of chromatin looping. *Cell*, **159**, 1665–1680.
27. Dixon, J.R., Jung, I., Selvaraj, S., Shen, Y., Antosiewicz-Bourget, J.E., Lee, A.Y., Ye, Z., Kim, A., Rajagopal, N., Xie, W. et al. (2015) Chromatin architecture reorganization during stem cell differentiation. *Nature*, **518**, 331–336.
 28. Lee, D.-S., Luo, C., Zhou, J., Chandran, S., Rivkin, A., Bartlett, A., Nery, J.R., Fitzpatrick, C., O'Connor, C., Dixon, J.R. et al. (2019) Simultaneous profiling of 3D genome structure and DNA methylation in single human cells. *Nat. Methods*, **16**, 999–1006.
 29. Gilbert, L.A., Horlbeck, M.A., Adamson, B., Villalta, J.E., Chen, Y., Whitehead, E.H., Guimaraes, C., Panning, B., Ploegh, H.L., Bassik, M.C. et al. (2014) Genome-scale CRISPR-mediated control of gene repression and activation. *Cell*, **159**, 647–661.
 30. Kearns, N.A., Pham, H., Tabak, B., Genga, R.M., Silverstein, N.J., Garber, M. and Maehr, R. (2015) Functional annotation of native enhancers with a Cas9-histone demethylase fusion. *Nat. Methods*, **12**, 401–403.
 31. Thakore, P.I., D'Ippolito, A.M., Song, L., Safi, A., Shivakumar, N.K., Kabadi, A.M., Reddy, T.E., Crawford, G.E. and Gersbach, C.A. (2015) Highly specific epigenome editing by CRISPR-Cas9 repressors for silencing of distal regulatory elements. *Nat. Methods*, **12**, 1143–1149.
 32. Fulco, C.P., Munschauer, M., Anyoha, R., Munson, G., Grossman, S.R., Perez, E.M., Kane, M., Cleary, B., Lander, E.S. and Engreitz, J.M. (2016) Systematic mapping of functional enhancer–promoter connections with CRISPR interference. *Science*, **354**, 769–773.
 33. Gasperini, M., Hill, A.J., McFaline-Figueroa, J.L., Martin, B., Kim, S., Zhang, M.D., Jackson, D., Leith, A., Schreiber, J., Noble, W.S. et al. (2019) A genome-wide framework for mapping gene regulation via cellular genetic screens. *Cell*, **176**, 377–390.
 34. Durand, N.C., Robinson, J.T., Shamim, M.S., Machol, I., Mesirov, J.P., Lander, E.S. and Aiden, E.L. (2016) Juicebox provides a visualization system for Hi-C contact maps with unlimited zoom. *Cell Systems*, **3**, 99–101.
 35. Robinson, J.T., Turner, D., Durand, N.C., Thorvaldsdóttir, H., Mesirov, J.P. and Aiden, E.L. (2018) Juicebox.js provides a cloud-based visualization system for Hi-C data. *Cell Systems*, **6**, 256–258.e251.
 36. Kerpedjiev, P., Abdennur, N., Lekschas, F., McCallum, C., Dinkla, K., Strobelt, H., Luber, J.M., Ouellette, S.B., Azhir, A., Kumar, N. et al. (2018) HiGlass: web-based visual exploration and analysis of genome interaction maps. *Genome Biol.*, **19**, 125.
 37. Jung, M., Krämer, E., Grzenkowski, M., Tang, K., Blakemore, W., Aguzzi, A., Khazaie, K., Chlichlia, K., von Blankenfeld, G., Kettenmann, H. et al. (1995) Lines of murine oligodendroglial precursor cells immortalized by an activated neu tyrosine kinase show distinct degrees of interaction with axons in vitro and in vivo. *Eur. J. Neurosci.*, **7**, 1245–1265.
 38. Oosterveen, T., Kurdija, S., Alekseenko, Z., Uhde, C.W., Bergsland, M., Sandberg, M., Andersson, E., Dias, J.M., Muhr, J. and Ericson, J. (2012) Mechanistic Differences in the Transcriptional Interpretation of Local and Long-Range Shh Morphogen Signaling. *Dev. Cell*, **23**, 1006–1019.
 39. Weider, M., Wegener, A., Schmitt, C., Küspert, M., Hillgärtner, S., Bösl, M.R., Hermans-Borgmeyer, I., Nait-Oumesmar, B. and Wegner, M. (2015) Elevated in vivo levels of a single transcription factor directly convert satellite glia into oligodendrocyte-like cells. *PLoS Genet.*, **11**, e1005008.
 40. Andersson, R. and Sandelin, A. (2020) Determinants of enhancer and promoter activities of regulatory elements. *Nat. Rev. Genet.*, **21**, 71–87.
 41. Emery, B. and Dugas, J.C. (2013) Purification of oligodendrocyte lineage cells from mouse cortices by immunopanning. *Cold Spring Harb Protoc.*, **2013**, 854–868.
 42. Dugas, J.C. and Emery, B. (2013) Purification of oligodendrocyte precursor cells from rat cortices by immunopanning. *Cold Spring Harb Protoc.*, **2013**, 745–758.
 43. Carpenter, A.E., Jones, T.R., Lamprecht, M.R., Clarke, C., Kang, I.H., Friman, O., Guertin, D.A., Chang, J.H., Lindquist, R.A., Moffat, J. et al. (2006) CellProfiler: image analysis software for identifying and quantifying cell phenotypes. *Genome Biol.*, **7**, R100.
 44. Morabito, S., Miyoshi, E., Michael, N., Shahin, S., Martini, A.C., Head, E., Silva, J., Leavy, K., Perez-Rosendahl, M. and Swarup, V. (2021) Single-nucleus chromatin accessibility and transcriptomic characterization of Alzheimer's disease. *Nat. Genet.*, **53**, 1143–1155.
 45. Nott, A., Holtman, I.R., Coufal, N.G., Schlachetzki, J.C.M., Yu, M., Hu, R., Han, C.Z., Pena, M., Xiao, J., Wu, Y. et al. (2019) Brain cell type-specific enhancer-promoter interactome maps and disease-risk association. *Science*, **366**, 1134–1139.
 46. The Roadmap Epigenomics Consortium (2015) Integrative analysis of 111 reference human epigenomes. *Nature*, **518**, 317–330.
 47. Cusanovich, D.A., Hill, A.J., Aghamirzaie, D., Daza, R.M., Pliner, H.A., Berletch, J.B., Filippova, G.N., Huang, X., Christiansen, L., DeWitt, W.S. et al. (2018) A single-cell atlas of in vivo mammalian chromatin accessibility. *Cell*, **174**, 1309–1324.
 48. Stansfield, J.C., Cresswell, K.G. and Dozmorov, M.G. (2019) multiHiCompare: joint normalization and comparative analysis of complex Hi-C experiments. *Bioinformatics*, **35**, 2916–2923.
 49. Yusa, K., Zhou, L., Li, M.A., Bradley, A. and Craig, N.L. (2011) A hyperactive piggyBac transposase for mammalian applications. *Proc. Natl. Acad. Sci.*, **108**, 1531–1536.
 50. Breunig, J.J., Levy, R., Antonuk, C.D., Molina, J., Dutra-Clarke, M., Park, H., Akhtar, A.A., Kim, G.B., Hu, X., Bannykh, S.I. et al. (2015) Ets factors regulate neural stem cell depletion and gliogenesis in Ras pathway glioma. *Cell Rep.*, **12**, 258–271.
 51. He, D., Marie, C., Zhao, C., Kim, B., Wang, J., Deng, Y., Clavairoly, A., Frah, M., Wang, H., He, X. et al. (2016) Chd7 cooperates with Sox10 and regulates the onset of CNS myelination and remyelination. *Nat. Neurosci.*, **19**, 678–689.
 52. Liu, Z., Yan, M., Liang, Y., Liu, M., Zhang, K., Shao, D., Jiang, R., Li, L., Wang, C., Nussenzweig, D.R. et al. (2019) Nucleoporin Seh1 interacts with Olig2/Brd7 to promote oligodendrocyte differentiation and myelination. *Neuron*, **102**, 587–601.
 53. Zhang, L., He, X., Liu, L., Jiang, M., Zhao, C., Wang, H., He, D., Zheng, T., Zhou, X., Hassan, A. et al. (2016) Hdac3 interaction with p300 histone acetyltransferase regulates the oligodendrocyte and astrocyte lineage fate switch. *Dev. Cell*, **36**, 316–330.
 54. He, D., Wang, J., Lu, Y., Deng, Y., Zhao, C., Xu, L., Chen, Y., Hu, Y.C., Zhou, W. and Lu, Q.R. (2017) lncRNA functional networks in oligodendrocytes reveal stage-specific myelination control by an lncOL1/Suz12 complex in the CNS. *Neuron*, **93**, 362–378.
 55. Zhao, C., Deng, Y., Liu, L., Yu, K., Zhang, L., Wang, H., He, X., Wang, J., Lu, C., Wu, L.N. et al. (2016) Dual regulatory switch through interactions of Tcf7l2/Tcf4 with stage-specific partners propels oligodendroglial maturation. *Nat. Commun.*, **7**, 10883.
 56. Ou, Z., Sun, Y., Lin, L., You, N., Liu, X., Li, H., Ma, Y., Cao, L., Han, Y., Liu, M. et al. (2016) Olig2-targeted G-protein-coupled receptor Gpr17 regulates oligodendrocyte survival in response to lysolecithin-induced demyelination. *J. Neurosci.*, **36**, 10560–10573.

57. Lopez-Anido, C., Sun, G., Koenning, M., Srinivasan, R., Hung, H.A., Emery, B., Keles, S. and Svaren, J. (2015) Differential Sox10 genomic occupancy in myelinating glia. *Glia*, **63**, 1897–1914.
58. Zhao, C., Dong, C., Frah, M., Deng, Y., Marie, C., Zhang, F., Xu, L., Ma, Z., Dong, X., Lin, Y. et al. (2018) Dual requirement of CHD8 for chromatin landscape establishment and histone methyltransferase recruitment to promote CNS myelination and repair. *Dev. Cell*, **45**, 753–768.e758.
59. Elbaz, B., Aaker, J.D., Isaac, S., Kolarzyk, A., Brugarolas, P., Eden, A. and Popko, B. (2018) Phosphorylation state of ZFP24 controls oligodendrocyte differentiation. *Cell Rep.*, **23**, 2254–2263.
60. Laitman, B.M., Asp, L., Mariani, J.N., Zhang, J., Liu, J., Sawai, S., Chapouly, C., Horng, S., Kramer, E.G., Mitiku, N. et al. (2016) The transcriptional activator Krüppel-like Factor-6 is required for CNS myelination. *PLoS Biol.*, **14**, e1002467.
61. Bujalka, H., Koenning, M., Jackson, S., Perreau, V.M., Pope, B., Hay, C.M., Mitew, S., Hill, A.F., Lu, Q.R., Wegner, M. et al. (2013) MYRF is a membrane-associated transcription factor that autoproteolytically cleaves to directly activate myelin genes. *PLoS Biol.*, **11**, e1001625.
62. Liu, J., Magri, L., Zhang, F., Marsh, N.O., Albrecht, S., Huynh, J.L., Kaur, J., Kuhlmann, T., Zhang, W., Slesinger, P.A. et al. (2015) Chromatin landscape defined by repressive histone methylation during oligodendrocyte differentiation. *J. Neurosci.*, **35**, 352–365.
63. Langmead, B. and Salzberg, S.L. (2012) Fast gapped-read alignment with Bowtie 2. *Nat. Methods*, **9**, 357–359.
64. Zhang, Y., Liu, T., Meyer, C.A., Eeckhoute, J., Johnson, D.S., Bernstein, B.E., Nusbaum, C., Myers, R.M., Brown, M., Li, W. et al. (2008) Model-based analysis of ChIP-Seq (MACS). *Genome Biol.*, **9**, R137.
65. Abdennur, N. and Mirny, L.A. (2019) Cooler: scalable storage for Hi-C data and other genomically labeled arrays. *Bioinformatics*, **36**, 311–316.